Anomalous x-ray diffraction measurements of long-range order in (001)-textured $L1_0$ FePtCu thin films

M. Maret,[1] C. Brombacher,[2] P. Matthes,[2] D. Makarov,[2,*] N. Boudet,[3] and M. Albrecht[2]

[1]*Laboratory of Science and Engineering of Materials and Processes, Grenoble Institute of Technology, Centre National de la Recherche Scientifique, Université Joseph Fourier, Boîte Postale No. 75, F-38402 Saint Martin d'Hères, France*

[2]*Institute of Physics, Chemnitz University of Technology, D-09107 Chemnitz, Germany*

[3]*Institut Néel, Centre National de la Recherche Scientifique, Université Joseph Fourier, Boîte Postale No. 166, 38042 Grenoble Cedex 9, France*

(Received 13 April 2012; revised manuscript received 2 July 2012; published 24 July 2012)

Thin films of $L1_0$-ordered $(Fe_{51}Pt_{49})_{100-x}Cu_x$ with (001) texture were obtained by rapid thermal annealing of FePt(5 nm$-t$)/Cu(t) bilayers deposited by magnetron sputtering at room temperature on thermally oxidized Si(001) substrates. The $L1_0$ long-range ordering fully described by two independent chemical order parameters was investigated by anomalous x-ray diffraction measurements performed at the Fe K and Pt L_{III} edges. These measurements reveal that Cu atoms are preferentially located on the Fe-rich (001) planes. Up to a Cu content of 9 at.%, the Cu addition favors $L1_0$ ordering particularly after annealing to 600 °C, giving rise to an increase in effective magnetic anisotropy. Beyond this composition, Cu atoms displace a large fraction of Fe atoms to the Pt-rich (001) planes, leading to a rapid decrease in magnetic anisotropy and saturation magnetization.

DOI: 10.1103/PhysRevB.86.024204 PACS number(s): 61.66.Dk, 68.55.−a, 68.35.−p, 75.50.Ss

I. INTRODUCTION

Intensive research activities have been devoted to (001)-oriented $L1_0$-ordered FePt alloy films due to their high perpendicular magnetocrystalline anisotropy (up to $\sim$10 MJ/m^3),[1] making them promising candidates as ultrahigh-density recording material or for sensor applications. During the past ten years, improvements have been achieved for decreasing the fabrication costs of (001)-oriented FePt films. One route was to grow FePt on thermally oxidized Si(100) wafers at room temperature and then to rapidly anneal the as-grown disordered fcc FePt films at high temperatures.[2,3] The annealing process promotes the formation of the $L1_0$ tetragonal phase with a strong (001) texture. In this case, the phase transformation might be driven by the anisotropic strain of the ordering transformation, which can easily occur on amorphous substrates.[4] Another important aspect is the lowering of the required annealing temperature to form $L1_0$-ordered films by alloying FePt with a third element, which, owing to its high mobility, enhances the ordering kinetics. Among candidate elements, Cu was demonstrated to lower substantially the order-disorder transformation temperature during postannealing of initially disordered films.[5–9] Furthermore, the addition of Cu decreases effectively the Curie temperature of the $L1_0$ phase,[10] making the ternary FePtCu alloy films attractive for future heat-assisted magnetic recording applications and allowing tailoring of the magnetic anisotropy values, which can be employed to create exchange-coupled composite thin-film systems.[11–14]

In binary (001)-oriented FePt films, it is well established that the uniaxial magnetic anisotropy increases with $L1_0$ long-range ordering.[15] The degree of long-range ordering is characterized by a single chemical order parameter S, which is defined by the difference of the rates of occupancy of Fe atoms $P^{\alpha}_{Fe} - P^{\beta}_{Fe}$ on the two sublattices α and β of the $L1_0$ structure. The α sublattice is described by the (0 0 0) and (1/2 1/2 0) sites, while the β sublattice is given by the (1/2 0 1/2) and (0 1/2 1/2) sites. Since the sum of the rates of occupancy on each sublattice is equal to 1, it follows that $S = S_{Fe} = -S_{Pt}$. In FePtCu ternary alloys a complete characterization of the chemical ordering requires the determination of two independent order parameters, for example, S_{Fe} and S_{Pt}, and since $\sum S_i = 0$, it follows that $S_{Cu} = -(S_{Fe} + S_{Pt})$. Therefore, the sign of S_{Cu} gives information about the preferential sites of Cu with respect to the alternating (001) planes of Fe and Pt in the $L1_0$ phase. In fact, since the ordered CuPt alloy does not adopt the $L1_0$ but the rhombohedral $L1_1$ structure characterized by Cu and Pt atoms positioned on alternating (111) planes,[16] the prediction of the Cu sites on the $L1_0$ tetragonal lattice is thus not straightforward. A previous work based on a comparison between first-principles band calculations and ultraviolet photoelectron spectroscopy experiments has indicated that Cu atoms tend to replace Fe atoms in the $L1_0$ FePt lattice.[17]

In this study, detailed x-ray diffraction experiments using tunable synchrotron radiation were performed on $L1_0$-ordered FePtCu thin films with various Cu content to quantify the chemical long-range-order (LRO) parameters and to highlight the impact of Cu addition on their structural and magnetic properties. Two samples series were investigated, which were obtained by rapid thermal annealing (RTA) at 600 °C and 800 °C, and the results were compared to binary FePt films. The anomalous x-ray diffraction measurements were performed at different energies close to the Fe K and Pt L_{III} absorption edges. By tuning the photon energy, the electronic contrast between the three atomic species varies, allowing the determination of two independent LRO parameters based on a graphical method.[18]

II. EXPERIMENT

Bilayers of $Fe_{51}Pt_{49}$(5 nm$-t$)/Cu(t) with a total thickness of 5 nm were dc magnetron sputter deposited at room temperature (with an Ar sputter pressure of 3.5×10^{-3} mbar) onto thermally oxidized Si(100) substrates. After deposition,

 ©2012 American Physical Society

the samples were transferred to a separate rapid thermal annealing chamber, where they were annealed for 30 s at temperatures of 600 °C and 800 °C under N_2 atmosphere (with an annealing rate of 400 °C/s). The Cu thickness t was varied between 0 and 1.2 nm and the Cu composition of the resulting ternary $(Fe_{51}Pt_{49})_{100-x}Cu_x$ alloy was determined by Rutherford backscattering spectrometry (RBS) to 0 and 21 at.% of Cu, respectively.

X-ray diffraction measurements were performed on the CRG-BM02 beamline at the European Synchrotron Radiation Facilities in Grenoble. For two series of FePtCu films after RTA at 600 °C and 800 °C, respectively, the (00l) reflections up to the sixth order, as well as the $(0\bar{2}2)$ and $(1\bar{1}1)$ reflections, were recorded using a photon energy of 18 keV ($\lambda = 0.689$ Å). Furthermore, for three samples processed by RTA at 800 °C, anomalous x-ray diffraction measurements of the (00l) reflections ($l = 1,2$) were carried out close to the Fe K (7.1 keV) and Pt L_{III} (11.5 keV) edges. For the magnetic characterization superconducting quantum interference device magnetometry was employed.

III. X-RAY DIFFRACTION RESULTS AND ANALYSIS OF ANOMALOUS MEASUREMENTS

Figure 1 shows typical (θ-2θ) scans and rocking curves recorded at 18 keV around the (00l) reflections of the $Fe_{47}Pt_{44}Cu_9$ film processed by RTA at 800 °C. The presence of the strong (001) superstructure reflection reflects the high degree of $L1_0$ ordering and (001) texture of this sample. From the full width at half maximum (FWHM) of the (00l) reflections, the perpendicular coherence length $L_\perp$, which is limited by the total film thickness, can be deduced. The $L_\perp$ values for the various FePtCu film samples are summarized in Table I. Note that the FePtCu samples processed by RTA at 800 °C reveal much larger values than compared to the total nominal film thickness of the as-grown bilayers, while

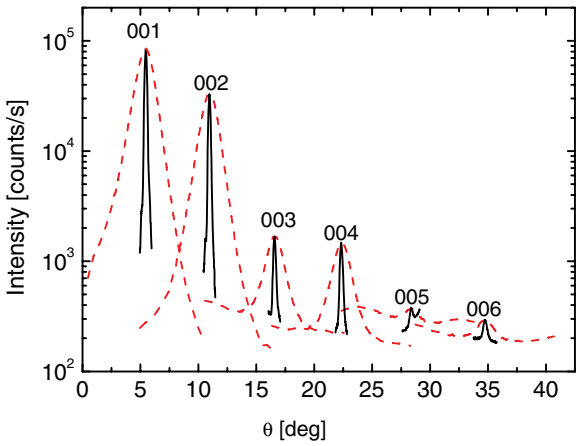

FIG. 1. (Color online) X-ray (θ-2θ) diffraction patterns (solid curves) and rocking curves (dashed curves) around the (00l) reflections recorded at 18 keV for the $Fe_{47}Pt_{44}Cu_9$ sample processed by RTA at 800 °C.

for those processed by RTA at 600 °C the values are close to the initial film thickness. Therefore, it is expected that strong dewetting and island formation occurs during the RTA treatment at 800 °C, while films processed by RTA at 600 °C stay continuous. This change in film morphology was confirmed by atomic force microscopy.[19] The vertical mosaic spread η_v and an estimate of the lateral coherent length $L_\parallel$ can be evaluated from the plot of $\Delta q_\parallel(00l)$ [deduced from the FWHM of the rocking curve around (00l)] versus q_{00l}: $\Delta q_\parallel(00l) = \eta_v q_{00l} + \frac{2\pi}{L_\parallel}$. These values are also given in Table I, showing a significant difference between the two sample series. It is clear from these data that RTA treatment at 800 °C improves the crystallinity of the $L1_0$ structure. Furthermore, for each sample the c lattice parameter of the $L1_0$ phase was extracted from the positions of the (00l) reflections. The differences between the values deduced for odd or even

TABLE I. Structural parameters of FePtCu films processed by RTA at 800 °C and 600 °C: a and c are lattice parameters of the $L1_0$ phase, $L_\perp$ and $L_\parallel$ are, respectively, perpendicular and lateral coherence lengths, η is the mosaicity, $B_{F\,(S)}$ is the Debye-Waller factor for the fundamental (superstructure) reflections, and S_i is the chemical order parameter for each element i. The errors on the last digits are in parentheses.

Samples	c/a (Å)	$L_\perp/L_\parallel$ (nm)/η (deg)	B_F/B_S (Å^2)	S_{Fe}	S_{Pt}	S_{Cu}
		Series 800 °C				
$Fe_{51}Pt_{49}$	3.73/3.90	11.2/120[a]/1.9(1)	1.4/2	0.79(1)	−0.79(1)	
$Fe_{49}Pt_{47}Cu_4$	3.68/3.91	9.1/85[a]/1.5(1)	1.7/2.3	0.78(4)	−0.83(2)	0.05(4)
$Fe_{47}Pt_{44}Cu_9$	3.63/3.92	8.8/220[a]/1.6(1)	1.4/2.1	0.75(4)	−0.87(2)	0.12(4)
$Fe_{44}Pt_{41}Cu_{15}$	3.6/3.92	13.7/220[a]/1.4(1)	1.3/1.9	0.68(5)	−0.85(2)	0.17(5)
$Fe_{44.5}Pt_{42.5}Cu_{13}$[b]						
$Fe_{41}Pt_{38}Cu_{21}$	3.58/3.92	16.5/160[a]/2.3(1)	1.6/1.0	0.64(5)	−0.84(2)	0.20(5)
$Fe_{43}Pt_{42}Cu_{15}$[b]						
		Series 600 °C				
$Fe_{51}Pt_{49}$	3.72/3.90	5/50[a]/2.3(1)	1.9/7.5	0.70(2)	−0.70(2)	
$Fe_{49}Pt_{47}Cu_4$	3.67/3.92	4.6/110[a]/2.5(2)	1.6/4.2	0.72(4)	−0.78(2)	0.06[c]
$Fe_{47}Pt_{44}Cu_9$	3.62/3.94	4.6/90[a]/2.7(2)	1.5/3.6	0.72(4)	−0.85(2)	0.13[c]
$Fe_{44}Pt_{41}Cu_{15}$	3.58/3.94	4.5/90[a]/3.0(2)	1.34/3.6			
$Fe_{41}Pt_{38}Cu_{21}$	3.54/3.94	4.5/20[a]/2.9(2)	1.3/1.9			

[a]Error of about 50%.
[b]Alloy composition deduced from the diffraction data analysis.
[c]The S_{Cu} value was chosen very close to that found for the corresponding alloy RTA processed at 800 °C.

l values do not exceed 0.015 Å, indicating that the growth of in-plane variants of the $L1_0$ phase is negligible. Therefore, the RTA treatment of the FePt/Cu bilayer leads exclusively to the formation of the out-of-plane $L1_0$ variant. Measurements of the $(0\bar{2}2)$ and $(1\bar{1}1)$ reflections yield the determination of the a lattice parameter. As summarized in Table I, it appears that the tetragonal distortion increases with Cu content and is more pronounced in the films processed by RTA at 600 °C. It is likely that the island formation, occurring for the films processed by RTA at 800 °C, releases partially the anisotropic elastic stress. The rocking curves around these reflections are flat, indicating that the films after RTA consist of (001)-oriented $L1_0$ grains randomly distributed in the substrate plane. This observation was further confirmed by transmission electron microscopy and electron backscatter diffraction.[19]

To determine the LRO parameter from the ratio of the integrated intensities between odd and even (00l) reflections, corrections for background (including fluorescence), sample absorption, Lorentz factor, and Debye-Waller attenuation factors have to be applied. The background level was removed by fitting all peaks with Gaussian functions. The absorption factor is given by $A(2\theta) = \frac{1}{2\mu_s}[1 - \exp(-\frac{2\mu_s d}{\sin\theta})]$, where μ_s is the linear attenuation factor and d is the total film thickness. For the Lorentz factor applied for a θ-2θ scan, we used an expression derived for samples with large mosaicity,[20] which is given by $L(2\theta) = \frac{f_v f_h}{\sin 2\theta}$. The $f_{v\,(h)}$ terms depend on the vertical (horizontal) sample mosaicity and beam collimation. For our experimental setup, in which the detector moves in the vertical plane, only f_v depends on θ and needs to be taken into account for the calculation of the LRO parameter; f_v is expressed by $[1 + 4\eta_v^2 \sin^2\theta/(\beta_M^2 + \beta_A^2)]^{-1/2}$, where β_M and β_A are the vertical collimations before and after the sample equal to 0.014 ° and 0.088 °, respectively. The integrated intensities of the (00l) peaks are thus related to the structure factor F_{00l} as

$$I_{(00l)} \propto |F_{00l}|^2 A(2\theta) L(2\theta) \exp\left(-\frac{B_{S\,(F)} \sin^2\theta}{\lambda^2}\right). \quad (1)$$

The two Debye-Waller factors $B_{S\,(F)}$ (S denotes superstructure and F denotes fundamental) describe the attenuation of the diffraction intensity due to the mean-square static displacements from the ideal lattice sites. They are extracted from the odd and even (00l) peaks, respectively, by plotting $\ln(\frac{I_{00l}}{AL|F_{00l}|^2})$ versus $\frac{\sin^2\theta}{\lambda^2}$ as described in Ref. 21. The slope of this function leads to the corresponding $B_{S\,(F)}$ values. The extracted values are given in Table I. For the determination of B_S in the ternary alloys, since the slope depends now on two independent parameters, we assume perfect $L1_0$ ordering such that S_{Fe} and S_{Pt} are equal to $2x_{Fe}$ and $-2x_{Pt}$ (x_i being the atomic fraction of element i). Note that this assumption will be discussed later based on the results of anomalous x-ray diffraction measurements. For the sample series processed by RTA at 800 °C, the B_F and especially the B_S values are smaller than the ones obtained for the sample series processed by RTA at 600 °C, again indicating the improved crystallinity of the $L1_0$ phase formed at 800 °C. It is also worth emphasizing that the largest values of $B_{S\,(F)}$ are obtained for the binary alloy processed by RTA at 600 °C, which can be related to the existence of a mixture of randomly oriented fcc A1 and (001)-oriented $L1_0$ grains as confirmed by transmission electron microscopy.[19]

As already mentioned, $L1_0$ ordering in binary alloys is described by a single order parameter $S_{Fe} = -S_{Pt}$, while for ternary alloys two independent parameters are required, i.e., S_{Fe} and S_{Pt} with $S_{Cu} = -(S_{Fe} + S_{Pt})$. For the binary alloys, S_{Fe} is deduced from the ratio of the integrated intensities of the superstructure and fundamental peaks corrected for absorption and Lorentz and Debye-Waller factors using Eq. (1) for $l = 1$ and 2. The order parameter is then expressed by

$$S_{Fe} = \sqrt{\frac{I_{001}|F_{002}|^2 A_{002} L_{002} \exp(-B_F \sin^2\theta_{002}/\lambda^2)}{I_{002}|F_{001}|^2 A_{001} L_{001} \exp(-B_S \sin^2\theta_{001}/\lambda^2)}}. \quad (2)$$

The expression of the structure factor of the (00l) fundamental reflections (even l) is given by

$$|F_{00l}|^2 = 16\left[\left(\sum_{i=1}^{2,3} x_i\left[f_i^0(00l) + f_i'\right]\right)^2 + \left(\sum_{i=1}^{2,3} x_i f_i''\right)^2\right], \quad (3)$$

which is valid for binary as well as for ternary alloys, where x_i is the atomic fraction of element i, $f_i^0(00l)$ is its normal coherent scattering factor dependent on the scattering vector $q_{00l} = 4\pi \sin\theta/\lambda$, and f_i' and f_i'' are, respectively, the real and imaginary parts of the anomalous scattering factor depending on the photon energy E.

For binary alloys, the expression of the structure factors of the (00l) superstructure reflections (odd l) is

$$|F_{00l}|^2 = 4S_{Fe}^2\left\{\left[f_{Fe}^0(00l) + f_{Fe}' - f_{Pt}^0(00l) - f_{Pt}'\right]^2 + (f_{Fe}'' - f_{Pt}'')^2\right\}. \quad (4)$$

For equiatomic composition the maximal value of S_{Fe} is equal to 1; otherwise it is $1 - |1 - 2x_{Fe}|$. For the two binary FePt samples, S_{Fe} was thus determined using Eq. (2). As expected, the chemical LRO parameter increases from 0.70 to 0.79 with increasing annealing temperature.

For ternary alloys, the superstructure $|F_{00l}|^2$ is expressed as a quadratic form of the two order parameters:

$$|F_{00l}|^2 = C_1 S_{Fe}^2 + C_2 S_{Pt}^2 + C_3 S_{Fe} S_{Pt} \quad (5)$$

with

$$C_1 = 4\left\{\left[f_{Fe}^0(00l) + f_{Fe}' - f_{Cu}^0(00l) - f_{Cu}'\right]^2 + (f_{Fe}'' - f_{Cu}'')^2\right\},$$
$$C_2 = 4\left\{\left[f_{Pt}^0(00l) + f_{Pt}' - f_{Cu}^0(00l) - f_{Cu}'\right]^2 + (f_{Pt}'' - f_{Cu}'')^2\right\},$$
$$C_3 = 8\left\{\left[f_{Fe}^0(00l) + f_{Fe}' - f_{Cu}^0(00l) - f_{Cu}'\right]\left[f_{Pt}^0(00l) + f_{Pt}' - f_{Cu}^0(00l) - f_{Cu}'\right] + (f_{Fe}'' - f_{Cu}'')(f_{Pt}'' - f_{Cu}'')\right\}.$$

The ratio of the intensities of superstructure and fundamental peaks leads to

$$|F_{001}|^2 = \frac{I_{001}|F_{002}|^2 A_{002} L_{002} \exp(-B_F \sin^2\theta_{002}/\lambda^2)}{I_{002} A_{001} L_{001} \exp(-B_S \sin^2\theta_{001}/\lambda^2)}. \quad (6)$$

Anomalous x-ray diffraction measurements performed at different energies in the vicinity of the Fe K and Pt L_{III} absorption edges allow one to change the C_i coefficients and $|F_{001}|^2$ values, owing to the energy dependence of the anomalous terms of the scattering factor. For each energy the solutions S_{Fe} and S_{Pt} of Eq. (5) are located on an ellipse whose

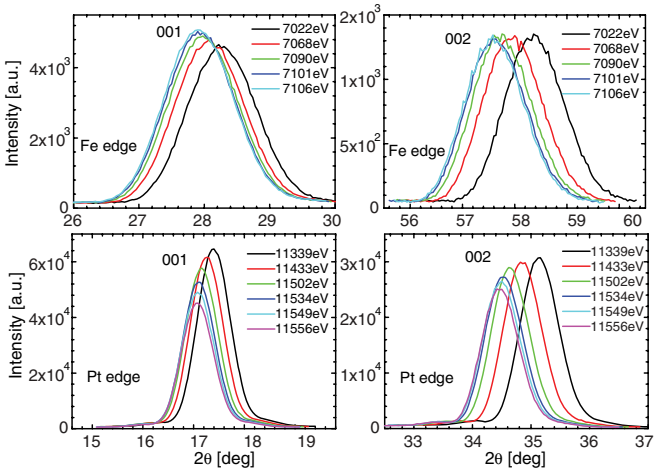

FIG. 2. (Color online) X-ray diffraction (θ-2θ) scans around the (001) and (002) reflections for the $Fe_{47}Pt_{44}Cu_9$ sample processed by RTA at 800 °C, recorded for different energies below the Fe K and Pt L_{III} absorption edges.

center is located at $S_{Fe} = S_{Pt} = 0$. The two LRO parameters are finally defined by the intersection points of the ellipses measured at different energies. This graphical method was already successfully applied to $L1_2$-ordered ternary alloys.[18]

However, due to the errors in the experimental values of $|F_{001}|^2$ and the weak energy dependence of the ellipse orientation (related to the C_i coefficients), ellipses measured at a single edge having similar orientation rarely intersect within the polygon of the allowed values. This polygon is limited to the region between the straight lines given by $S_{Fe} = 2x_{Fe}$, $S_{Pt} = -2x_{Pt}$, and $S_{Fe} + S_{Pt} = -2x_{Cu}$ (valid for $x_i < 0.5$). Therefore, carrying out anomalous x-ray diffraction measurements at both Fe K and Pt L_{III} edges leads to significant changes of the ellipse orientation and drastically increases the probability that ellipses measured at different edges intersect in the region of allowed solutions.

Figure 2 shows the (001) and (002) reflections of the $Fe_{47}Pt_{44}Cu_9$ film processed by RTA at 800 °C (same alloy as in Fig. 1), measured at different energies slightly below the Fe K and Pt L_{III} edges. At both edges the intensity variation of the (001) peak is more pronounced than that of the (002) peak. These changes are larger at the Pt edge due to the larger anomalous effect as shown in Fig. 3.

The S_{Fe} and S_{Pt} parameters were determined by drawing the ellipses described by Eq. (5), in which for each energy the experimental values of $|F_{001}|^2$ are deduced from Eq. (6). Assuming that Pt atoms are preferentially on the β sublattice, i.e., S_{Pt} defined by $P_{Pt}^{\alpha} - P_{Pt}^{\beta}$ is negative, for S_{Pt} ranging from -1 to 0 the corresponding values of S_{Fe} are the positive solutions of the quadratic function given by Eq. (5). For the $Fe_{47}Pt_{44}Cu_9$ alloy, the positive S_{Fe} solutions ranging from 0 to 1 are thus found in a narrow S_{Pt} range and are represented by the parts of ellipses depicted in Fig. 4. It is worth emphasizing the variation of these curves with the photon energy, which is well marked, by changing from the Fe edge to Pt one. The intersection between all curves defines the gray diamond, but only the region close to its top right corner belongs to the purple polygon of the allowed values. The center of

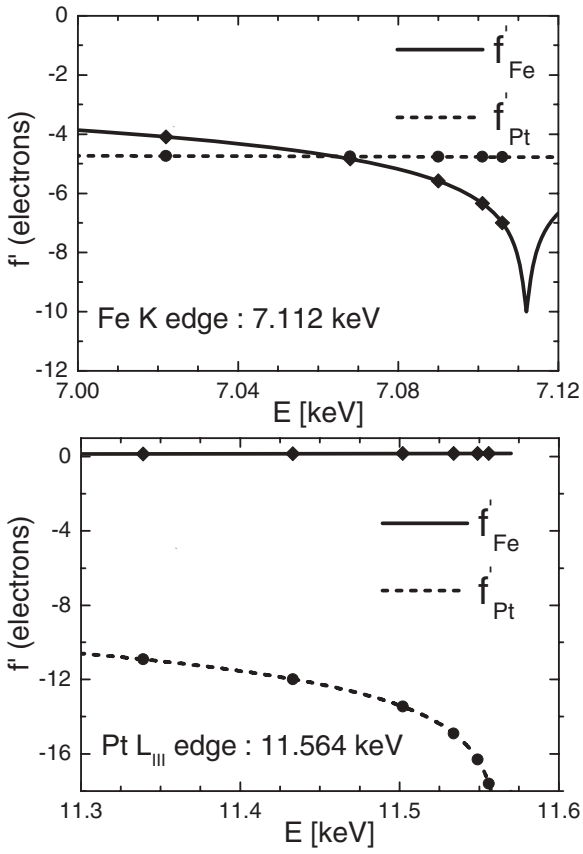

FIG. 3. Real parts f_i' of the anomalous terms of the Fe and Pt atomic form factor in the vicinity of the Fe K and Pt L_{III} absorption edges. Symbols mark the energies used in the experiment.

this common zone leads to a satisfying solution given by $S_{Pt} = -0.87$, $S_{Fe} = 0.75$, and $S_{Cu} = 0.12$. Let us note that this zone is limited by the four ellipses obtained at energies of 7.068, 7.090, 11.339, and 11.433 keV, for which the ratio $|F_{002}|^2 A_{002} L_{002} \exp(-B_F \sin^2\theta_{002}/\lambda^2)/I_{002}$ is identical at each

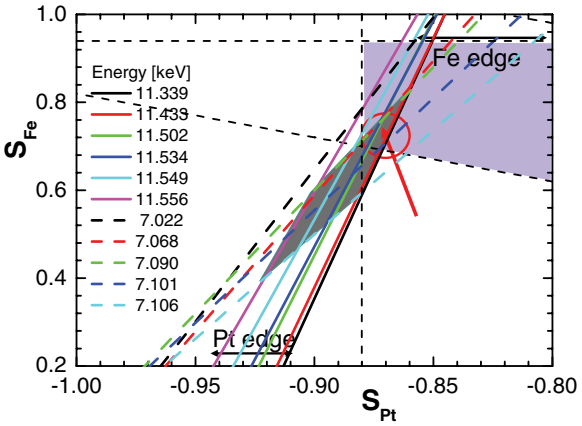

FIG. 4. (Color online) Graphical determination of the two LRO parameters S_{Fe} and S_{Pt} for the $Fe_{47}Pt_{44}Cu_9$ sample RTA processed at 800 °C. A reliable solution ($S_{Pt} = -0.87$, $S_{Fe} = 0.75$, and $S_{Cu} = 0.12$) is given by the center of the common zone between the gray diamond and the purple polygon of the allowed solutions with respect to the alloy composition.

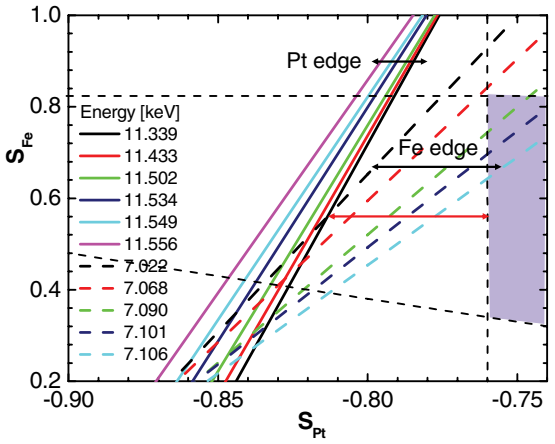

FIG. 5. (Color online) Graphical determination of the two LRO parameters S_{Fe} and S_{Pt} for the $Fe_{41}Pt_{38}Cu_{21}$ sample RTA processed at 800 °C by taking this alloy composition deduced from RBS for the calculation of $|F_{002}|^2$. The intersection between the ellipses obtained for $E = 7.022$ and 11.33 keV is the closest one from the purple area and leads to a value of S_{Pt} of −0.82 (see also the text).

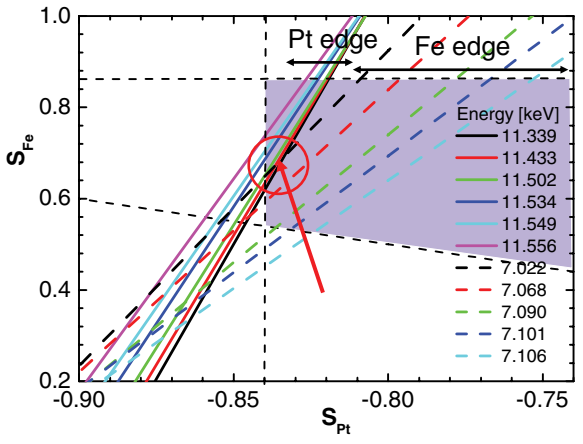

FIG. 6. (Color online) Graphical determination of the two LRO parameters S_{Fe} and S_{Pt} for the $Fe_{41}Pt_{38}Cu_{21}$ sample after RTA at 800 °C, but now assuming a modified composition of $Fe_{43}Pt_{42}Cu_{15}$ for the calculation of $|F_{002}|^2$. For this composition, one intersection between ellipses of the two different edges belongs to the purple region, leading to $S_{Pt} = -0.84$, $S_{Fe} = 0.64$, and $S_{Cu} = 0.2$.

edge, indicating that the beam characteristics and footprint on the sample were identical during these measurements. Furthermore, this set of chemical order parameters is in agreement with the $|F_{001}|^2$ value measured at 18 keV. The use of these LRO parameters in Eq. (5) to evaluate the Debye-Waller factor from the series of the superstructure reflections measured at 18 keV leads to a value of B_s equal to 2.08 Å^2, which is very close to the value assuming perfect $L1_0$ order. Thus, for the ternary $Fe_{47}Pt_{44}Cu_9$ alloy film, 99% of Pt atoms are distributed on the β sublattice with a S_{Pt} value very close to the maximal value. Ninety percent of Fe atoms and 83% of Cu are located on the α sublattice. Therefore, the Cu atoms are preferentially placed on the Fe-rich (001) planes.

For the film of $Fe_{41}Pt_{38}Cu_{21}$ processed by RTA at 800 °C, the ellipses (Fig. 5) were calculated using the given alloy composition as determined by RBS. It turns out that no intersection between the ellipses belongs to the region of the allowed solutions. The closest intersection from this region leads to a S_{Pt} value of 0.82, corresponding to a difference in Pt composition of 3%.

This discrepancy cannot be attributed to an experimental error in composition evaluation. Therefore, it is believed that during the fast annealing process a fraction of the Cu atoms was not intermixed with the FePt alloy and is located at the grain boundaries. By increasing the Pt composition from 38 at. % to 42 at.% and Fe to 43 at.%, resulting in a modified composition of $Fe_{43}Pt_{42}Cu_{15}$, a few intersections are now found marked in the purple region of Fig. 6. The solution indicated by the red arrow corresponds to $S_{Pt} = -0.84$ (maximal value), $S_{Fe} = 0.64$, and $S_{Cu} = 0.2$. Thus Cu atoms are again located preferentially on the Fe-rich (001) planes. Based on this tendency for Cu sites, also ordering parameters for the two remaining FePtCu alloy films processed by RTA at 800 °C, consistent with the value of $|F_{00l}|^2$ measured at 18 keV, were calculated. The corresponding values are summarized in Table I. For two ternary alloy films processed by RTA at 600 °C with low Cu content, the order parameters were deduced from the 18-keV measurement data by assuming values for S_{Cu} similar to those of the corresponding alloys after RTA at 800 °C. As already observed for the binary alloy, the S_{Fe} and S_{Pt} values are always smaller than those determined for the corresponding films after RTA at 800 °C, which can be attributed to a lower atomic mobility.

IV. DISCUSSION

To emphasize the role of Cu on the $L1_0$-ordering process, the normalized LRO parameters given by $|S_i|/2x_i$ versus the Cu content are presented in Fig. 7. For the samples processed by RTA at 800 °C, the normalized Pt order parameter increases with Cu content, reaching its maximal value for a Cu content of 9 at. %, while the normalized Fe order parameter remains almost constant. Due to larger uncertainties on the Cu order

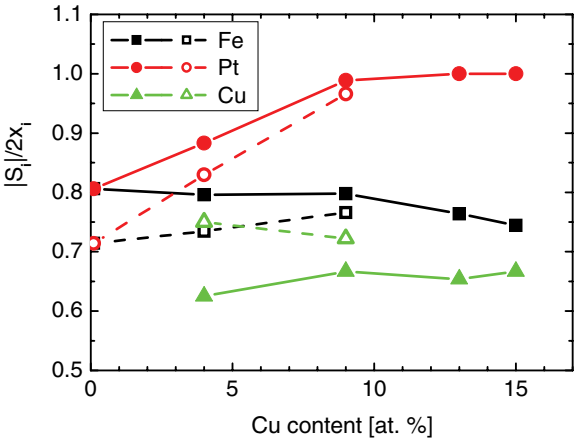

FIG. 7. (Color online) Chemical long-range-order parameters S_i normalized with respect to the maximal values given by $2x_i$ as a function of the Cu composition deduced from the x-ray data analysis for the FePtCu sample series processed by RTA at 800 °C (closed symbols) and for three FePtCu samples processed by RTA at 600 °C (open symbols).

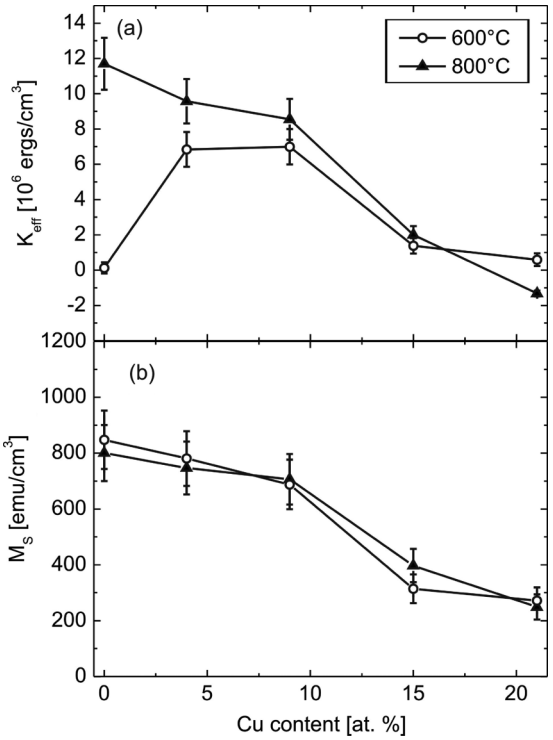

FIG. 8. Change of (a) the effective magnetic anisotropy K_{eff} and (b) the saturation magnetization M_s as a function of the Cu content (value determined by RBS) for FePtCu films processed by RTA at 600 °C and 800 °C.

parameter, the change of its normalized parameter is not significant. Beyond 9 at.%, the decrease of the normalized Fe order parameter becomes evident, indicating clearly that Cu atoms displace more and more Fe atoms on the Pt-rich planes. Such a redistribution of atoms in the tetragonal phase gives rise to a decrease in number of FePt bonds along the tetragonal axis, which in turn will strongly affect the magnetic anisotropy. Figure 8(a) shows the values of the effective perpendicular magnetic anisotropy K_{eff}, deduced from the area difference between the parallel and perpendicular hysteresis loops measured at 300 K. The K_{eff} value of the binary alloy reaches up to 1.2×10^6 erg/cm^3, which is in agreement with the highest degree of chemical order for Fe atoms. The addition of Cu leads to a decrease of K_{eff} as expected from the lowering of the S_{Fe} parameter, which in turn leads also to a reduction of the saturation magnetization M_s, as shown in Fig. 8(b). It is worth noting that the increase of the tetragonal distortion (c/a ratio; see Table I) with Cu addition could also lead to a decrease of magnetocrystalline anisotropy, as predicted by first-principles calculations applied to a perfectly ordered $L1_0$ FePt alloy.[22]

In contrast, for the sample series processed by RTA at 600 °C, the addition of Cu first enhances the perpendicular magnetic anisotropy due to the increased $L1_0$-ordered volume fraction. Beyond 9 at.%, again the redistribution of atoms in the tetragonal phase leads to a decrease of K_{eff} mainly given by the reduction of the saturation magnetization as shown in Fig. 8.

V. CONCLUSION

For $L1_0$ FePtCu alloy films, obtained after rapid thermal annealing of polycrystalline FePt(5 nm$-t$)/Cu(t) bilayers, anomalous x-ray diffraction measurements performed at the Fe K and Pt L_{III} edges have clearly shown that Cu atoms replace preferentially Fe atoms on the (001) Fe-rich planes in the $L1_0$ phase. While up to a Cu content of 9 at.% the Cu atoms play an important role in the formation of the $L1_0$ phase with (001) texture and consequently in the development of strong perpendicular magnetic anisotropy, above 9 at.% Cu the displacement of more and more Fe atoms to the (001) Pt-rich planes leads to a strong decrease of perpendicular magnetic anisotropy.

ACKNOWLEDGMENTS

Allocation of beamtime on the French Collaborating Research Group (CRG) BM02 beamline at the European Synchrotron Radiation Facilities is gratefully acknowledged. The authors thank the CRG BM02 staff for their technical help and J. P. Simon (Laboratory of Science and Engineering of Materials and Processes) for enlightening discussions in the anomalous data analysis. Financial support was provided by the French Minister of Foreign and European Affairs (Partenariats Hubert Curien Procope) and the Deutsche Akademischer Austauschdienst (Grant No. 50077059).

*Present address: Institute for Integrative Nanosciences, Leibniz Institute for Solid State and Materials Research, D-01069 Dresden, Germany.

[1] J. U. Thiele, L. Folks, M. F. Toney, and D. K. Weller, J. Appl. Phys. **84**, 5686 (1998).
[2] M. L. Yan, X. Z. Li, L. Gao, S. H. Liu, D. J. Sellmyer, R. J. M. van de Veerdonk, and K. W. Wierman, Appl. Phys. Lett. **83**, 3332 (2003).
[3] Y. Shao, M. L. Yan, and D. J. Sellmyer, J. Appl. Phys. **93**, 8152 (2003).
[4] J. S. Kim, Y. M. Koo, B. J. Lee, and S. R. Lee, J. Appl. Phys. **99**, 053906 (2006).
[5] T. Maeda, T. Kai, A. Kikitsu, T. Nagase, and J. I. Akiyama, Appl. Phys. Lett. **80**, 2147 (2002).
[6] Y. K. Takahashi, M. Ohnuma, and K. Hono, J. Magn. Magn. Mater. **246**, 259 (2002).
[7] S. D. Willoughby, J. Appl. Phys. **95**, 6586 (2004).
[8] M. L. Yan, Y. F. Xu, and D. J. Sellmyer, J. Appl. Phys. **99**, 08G903 (2006).
[9] W. Y. Zhang, H. Shima, F. Takano, H. Akinaga, X. Z. Yu, T. Hara, W. Z. Zhang, K. Kimoto, Y. Matsui, and S. Nimori, J. Appl. Phys. **106**, 033907 (2009).
[10] D. C. Berry and K. Barmak, J. Appl. Phys. **102**, 024912 (2007).
[11] V. Bonanni, Y. Y. Fang, R. K. Dumas, C. L. Zha, S. Bonetti, J. Nogués, and J. Åkerman, Appl. Phys. Lett. **97**, 202501 (2010).
[12] D. Makarov, J. Lee, C. Brombacher, C. Schubert, M. Fuger, D. Suess, J. Fidler, and M. Albrecht, Appl. Phys. Lett. **96**, 062501 (2010).

[13]R. K. Dumas, Y. Fang, B. J. Kirby, C. Zha, V. Bonanni, J. Nogués, and J. Åkerman, Phys. Rev. B **84**, 054434 (2011).
[14]Y. Fang, R. K. Dumas, C. L. Zha, and J. Åkerman, IEEE Magnetics Letters **2**, 5500104 (2011)
[15]K. Barmak, J. Kim, L. H. Lewis, K. R. Coffey, M. F. Toney, A. J. Kellock, and J.-U. Thiele, J. Appl. Phys. **98**, 033904 (2005).
[16]C. Barrett and T. B. Massalski, *Structure of Metals*, 3rd ed., International Series on Materials Science and Technology Vol. 35 (Pergamon, Oxford, 1980).
[17]T. Kai, T. Maeda, A. Kikitsu, J. Akiyama, T. Nagase, and T. Kishi, J. Appl. Phys. **95**, 609 (2004).
[18]A. Marty, M. Bessière, F. Bley, Y. Calvayrac, and S. Lefebvre, Acta Metall. Mater. **38**, 345 (1990).
[19]C. Brombacher, H. Schletter, M. Daniel, P. Matthes, N. Jöhrmann, M. Maret, D. Makarov, M. Hietschold, and M. Albrecht, J. Appl. Phys. (to be published).
[20]J. D. Axe and J. B. Hastings, Acta Crystallogr. Sect. A **39**, 593 (1983).
[21]H. Berg and J. B. Cohen, Metall. Trans. **3**, 1797 (1972).
[22]Z. Lu, R. V. Chepulskii, and W. H. Butler, Phys. Rev. B **81**, 094437 (2010).